

## Influence of the chemical composition of the porous matrix and sintering atmosphere on the luminescent properties of bismuth-containing composites

© M.A. Girsova, T.V. Antropova, G.F. Golovina, I.N. Anfimova, L.N. Kurilenko

Grebenschikov Institute of Silicate Chemistry RAS,  
199034 Saint Petersburg, Russia

e-mail: girsovama@yandex.ru

Received August 18, 2022

Revised November 2, 2022

Accepted November 7, 2022

The spectral-optical and luminescence properties of bismuth-containing composite materials based on matrices of high-silica porous glasses are investigated. Luminescence spectra, luminescence excitation spectra, infrared transmission spectra ( $8000\text{--}4000\text{ cm}^{-1}$ ) depending on the composition of different types of matrices and sintering atmosphere (nitrogen, argon) of bismuth-containing composite materials were examined. It was found that the samples of bismuth-containing composite materials are characterized by UV ( $\lambda_{\text{em}} = 350\text{ nm}$ ), blue-green ( $\lambda_{\text{em}} = 410\text{--}550\text{ nm}$ ) and orange-red ( $\lambda_{\text{em}} = 600\text{--}725\text{ nm}$ ) luminescence due to the presence of various bismuth active centers. The analysis of the spectra obtained by near-infrared spectroscopy demonstrates the formation of  $\text{Bi}^{2+}$  dimers of bismuth and bismuth active centers associated with silicon.

**Keywords:** Bismuth-containing composite materials, high-silica porous glass, near-infrared spectroscopy, luminescence, bismuth active centers.

DOI: 10.21883/EOS.2023.01.55521.4040-22

### Introduction

Bismuth-containing silicate glasses are of interest due to the fact that they have luminescence in a wide spectral range from the near UV region to the near IR region, including the range of  $1150\text{--}1800\text{ nm}$ , due to the presence of various bismuth active centers (BAC) [1–20]. Various methods are known for producing bismuth-containing glassy optical materials of silicate, aluminosilicate, phosphate-silicate systems with luminescent properties. Such methods of production include the method of quenching the melt (conventional melting-quenching technique) [2,3,13,14,18], the powder-in-tube technology [10,12,17], the Modified Chemical Vapor Deposition method — MCVD) [10,11,17]. These methods for producing bismuth-containing glasses involve synthesis under high temperature conditions  $\sim 1050\text{--}2200^\circ\text{C}$  [2,3,10–14,17], which does not allow to regulate the degree of oxidation of bismuth and, consequently, the nature of BAC and the nature of luminescence. In addition, the synthesis of materials at high temperature leads to an increase in energy consumption. When using traditional synthesis methods, there are restrictions on the concentrations of bismuth introduced into silicate glass (in terms of oxide  $\text{Bi}_2\text{O}_3$ ): it usually does not exceed 0.1 mas.% when using powder-in-tube and MCVD methods [10,12] and 2 mol.% when synthesizing glasses by cooking from a charge [2,13,14].

Thus, an important task is to select the temperature-time modes of synthesis, as well as the type and morphology of the glass matrix, in which it is possible to effectively control

the formation and distribution of BAC with a certain degree of oxidation in nanoscale structures, avoiding the effects of clustering and concentration quenching.

A promising method for producing a luminescent bismuth-containing material based on matrices of high-silica porous glasses, into which bismuth compounds are introduced from water-salt solutions, is devoid of these disadvantages [1,4–9,15,16]. Bismuth-containing materials based on porous silicate matrices have photoluminescence in a wide range from blue-green to near-IR spectral range due to the presence of various BAC in glasses, including  $\text{Bi}^{3+}$ -,  $\text{Bi}^{2+}$ -,  $\text{Bi}^+$ -centers. It should be noted that this production technology allows to vary widely the parameters of the porous matrix itself, the concentration of bismuth introduced into the glass, to select the sintering atmosphere (oxidative, reducing, inert) and temperature-time synthesis modes [1,4–9,15,16].

In addition to selecting the morphology of the glass matrix for the manufacture of bismuth-containing glassy photoluminophores with improved luminescent properties, it is necessary to take into account the influence of the chemical composition of the glass. It is known that the introduction of phosphorus into the silicate matrix leads to an increase in the degree of reduction of bismuth in glass, as indicated by the darkening of the glasses (from brown to black) as the concentration of phosphorus increases [1]. Introduction of additional impurities in the form of  $\text{P}_2\text{O}_5$  or ions F at the level of fractions or several mass percent leads to a significant change in luminescence spectra compared to bismuth-containing silicate glasses without additional

alloying additives (BAC-Si) [10,17–20]. The peculiarity of the BAC formed in phosphorosilicate glasses (BAC-P) is that they are characterized by significant Stokes shifts of most lines, which indicates a significant influence of the electron-phonon interaction compared to the VAC-Si [10,17,20]. BAC-P also differ from BAC-Si by a much stronger dependence of the luminescence spectrum on the excitation wavelength for some luminescence bands [10,17].

In this paper, the influence of the chemical composition of matrices made of high-silica porous glasses and the sintering atmosphere of bismuth-containing composite materials on their spectral-optical and luminescent properties in the UV and visible spectral ranges is investigated. The choice of sintering atmosphere (nitrogen — reducing, argon — inert) is due to the fact that the nature of the coexistence of bismuth oxides ( $\text{BiO}_2$ ,  $\text{BiO}$ ,  $\text{Bi}_2\text{O}_3$ ,  $\text{Bi}_2\text{O}_5$ ) varies depending on the atmosphere (nitrogen/argon) and the sintering temperature, and the concentration of various BAC directly depends on the values of the equilibrium partial pressures of bismuth oxides [21,22].

## Characteristics of objects and research methods

The objects of the study were samples of bismuth-containing composite materials (BCM) in the form of rectangular plane-parallel plates (size  $5-25 \times 5-15 \times 1.5 \pm 0.15$  mm). BCM samples were synthesized by impregnation of matrices of high-silica porous glasses (PG-matrix) in aqueous salt solutions of bismuth nitrate pentahydrate with subsequent heat treatment in accordance with the procedure used in [4–8]. For the synthesis of BCM, PG-matrices without additives (hereinafter PG 8V-NT) and with small additives  $\text{P}_2\text{O}_5$  and fluoride ions (hereinafter PG-NFF) were used, manufactured according to the method [23]. The PG 8V-NT and PG-NFF matrices used have the following pore parameters: porosity  $W = 30\%$  and  $W = 30\%$ , the pore specific surface area (SA),  $S_{\text{ud.}} = 200 \text{ m}^2/\text{g}$  and  $S_{\text{ud.}} = 55 \text{ m}^2/\text{g}$ , the average pore diameter  $D = 3-5$  nm and  $D = 12$  nm respectively [23]. Two types of quartzoid glasses QG-8V-NT and QG-NFF, which do not contain bismuth, were made as comparison samples. The compositions of PG-matrices and QG samples are given in [4,23,24]. According to chemical analysis, the studied samples of BCM based on PG-8V-NT and PG-NFF matrices contain (in mas%) (1.13–1.18)  $\text{Bi}_2\text{O}_3$  and (1.78–1.96)  $\text{Bi}_2\text{O}_3$  respectively.

Studies of BCM in comparison with QG by near-IR spectroscopy (Fig. 1) were performed at room temperature using a spectrophotometer FSM-2211 in the frequency range  $8000-4000 \text{ cm}^{-1}$  with a spectral resolution of  $2 \text{ cm}^{-1}$ . Measurements were carried out on samples of BCM in the form of plane-parallel plates with a thickness of  $1.50 \pm 0.15$  mm.

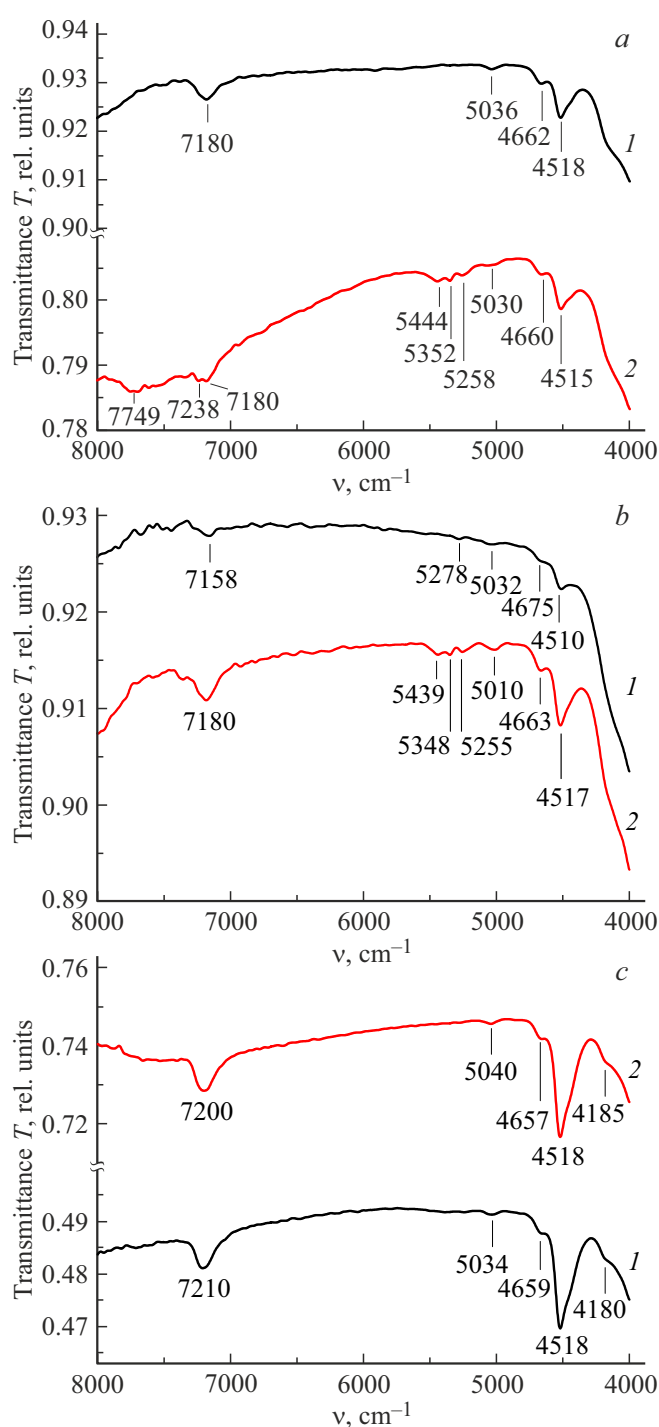


**Figure 1.** IR spectra at 300 K QG (1) and BCM (2) based on PG-NFF depending on the sintering atmosphere: argon (a), nitrogen (b); BCM based on PG-8V-NT (c) depending on the sintering atmosphere: argon (1), nitrogen (2). Heat treatment at  $900^\circ\text{C}$ .

The excitation spectra of the BCM luminescence at  $\lambda_{\text{em}} = 600$  nm (Fig. 2) and the BCM luminescence spectra at  $\lambda_{\text{ex}} = 280$  nm (Fig. 3) were measured on samples (in the form of plane-parallel plates with a thickness of  $1.50 \pm 0.15$  mm) at room temperature using an optical

Absorption bands (in the range of 8000–4000  $\text{cm}^{-1}$ ) found in quartzoid glasses and bismuth-containing composite materials depending on their production conditions

Designation of glasses and composites	Position of absorption bands, $\text{cm}^{-1}$									
QG 8V-NT ( $875 \pm 5^\circ\text{C}$ , air) [25]		7238	7176						4665	4522
BCM 8V-NT ( $875 \pm 5^\circ\text{C}$ , air) [25]		7218	7182						4663	4522
QG NFF ( $870 \pm 5^\circ\text{C}$ , air) [24]			7176						4663	4520
BCM NFF ( $870 \pm 5^\circ\text{C}$ , air) [24]			7168						4667	4524
QG NFF ( $890 \pm 10^\circ\text{C}$ , Ar)			7180					5036	4662	4518
BCM NFF ( $890 \pm 10^\circ\text{C}$ , Ar)	7749	7238	7180	5444	5352	5258		5030	4660	4515
BCM 8V-NT ( $890 \pm 10^\circ\text{C}$ , Ar)		7210						5034	4659	4518
QG NFF ( $890 \pm 10^\circ\text{C}$ , $\text{N}_2$ )			7158			5278		5032	4675	4510
BCM NFF ( $890 \pm 10^\circ\text{C}$ , $\text{N}_2$ )			7180	5439	5348	5255		5010	4663	4517
BCM 8V-NT ( $890 \pm 10^\circ\text{C}$ , $\text{N}_2$ )		7200						5040	4657	4518

spectrofluorimeter FLSP920 (Edinburgh Instruments) with a spectral resolution of 10 nm. The source of excitation was a xenon lamp with a power of 200 W. With the help of a monochromator, an excitation line was isolated from the radiation spectrum of the lamp. The range of excitation wavelengths was limited to the range from 200 to 850 nm. The test sample was positioned in such a way that the incident exciting radiation was perpendicular to the plane of the sample surface. The registration of visible and IR luminescence was carried out by Hamamatsu photoelectronic multipliers in a perpendicular direction with respect to the direction of the exciting radiation. The spectral resolution in the experiments on the measurement of excitation and luminescence spectra was selected based on the properties of the samples and was regulated by the size of the monochromator slots (from 4 to 10 nm).

Luminescence spectra of QG-8V-NT, QG-NFF, BCM at  $\lambda_{\text{ex}} = 280 \text{ nm}$  and  $\lambda_{\text{ex}} = 350 \text{ nm}$  (Figs. 4 and 5) were measured on samples (in the form of plane-parallel plates with a thickness of  $1.50 \pm 0.15 \text{ mm}$ ) at room temperature using an optical spectrofluorimeter RF 6000 (SHIMADZU Corp.; excitation source — xenon lamp 150 W, spectral slit width 1.5–3.0 nm).

## Research results

Fig. 1 shows the IR transmission spectra of QG and BCM in the frequency range 8000–4000  $\text{cm}^{-1}$  depending on the chemical composition of the PG-matrix (PG 8V-NT or PG-NFF) and the sintering atmosphere (nitrogen, argon). The table shows the absorption bands found in QG 8V-NT, QG-NFF and BCM in comparison with the previously obtained data [25,26].

Two groups of fundamental bands at 4675–4657 and 4524–4510  $\text{cm}^{-1}$  were found in all the QG and BCM, regardless of the composition of the PG-matrix and the sintering atmosphere. Additional bands in four frequency regions are characteristic for QG 8V-NT and BCM based on PG 8V-NT at 7238–7200, 7182–7176, 5040–5034, 4185–4180  $\text{cm}^{-1}$ . In BCM based on PG-

NFF and QG-NFF, additional bands were found at 7749, 7238, 7180–7158, 5444–5439, 5352–5348, 5278–5255, 5036–5010, 4182  $\text{cm}^{-1}$ .

It can be seen that there are no differences in the position of absorption bands in QG 8V-NT and BCM based on PG 8V-NT or PG-NFF (air), but the influence of the chemical composition of the matrix was found, which manifests itself in the appearance of additional bands at 7238–7218 and 4182  $\text{cm}^{-1}$ . The influence of the sintering atmosphere (air/ $\text{N}_2$ /Ar) in BCM based on PG 8V-NT was detected only in comparison ( $\text{N}_2$ /Ar) with the air atmosphere. In the case of QG and BCM based on PG-NFF (Table, Fig. 1), the influence of two factors is traced by the position of the absorption bands, namely the influence of the sample type (QG or BCM) and (in the case of BCM) the influence of the sintering atmosphere (air,  $\text{N}_2$  or Ar), which turns out to be more significant compared to BCM based on PG 8V-NT.

Observed weak bands at 5040–5010  $\text{cm}^{-1}$  ( $\sim 1984$ – $1996 \text{ nm}$ ) and at 4675–4657  $\text{cm}^{-1}$  ( $\sim 2139$ – $2147 \text{ nm}$ ) can be attributed to water molecules co-ordinatively bound to impurity boron atoms and to  $\nu(\text{B}^{\text{III}}\text{--OH})$  respectively [23,25,26]. The bands at 4522–4510  $\text{cm}^{-1}$  ( $\sim 2211$ – $2217 \text{ nm}$ ) are most likely related to stretching vibrations of OH groups ( $\nu(\text{OH})$ ), to bending vibrations of Si–OH-groups ( $\delta(\text{Si--OH})$ ), to the stretching vibrations of Na–OH groups ( $\nu(\text{Na--OH})$ ), are associated with a combination of bending and stretching Si–OH-groups ( $(\delta + \nu)\text{Si--OH}$ ) [23,25,26].

Additional low-intensity bands observed in BCM based on PG-NFF ( $\text{N}_2$ /Ar) at 5444 ( $\sim 1837$ ), 5439 ( $\sim 1839$ ), 5352 ( $\sim 1868$ ) and 5348  $\text{cm}^{-1}$  ( $\sim 1870 \text{ nm}$ ), can be attributed to a combination of stretching and bending vibrations of Si–OH groups ( $(\nu + \delta)\text{Si--OH}$ ) [27]. At QG-NFF ( $\text{N}_2$ ) and BCM based on PG-NFF ( $\text{N}_2$ /Ar) bands were detected at 5278 ( $\sim 1895$ ), 5258 ( $\sim 1902$ ) and 5255  $\text{cm}^{-1}$  ( $\sim 1903 \text{ nm}$ ), they may relate to the absorption of hydroxyl groups and water molecules adsorbed on the surface, as well as a combination of bending and stretching vibrations of water ( $(\delta + \nu)\text{H}_2\text{O}$ ) [23,25,26].

Most QG and BCM have found fundamental bands at 7238–7200 and 7182–7158  $\text{cm}^{-1}$ . Bands in the frequency range 7238–7200  $\text{cm}^{-1}$  ( $\sim 1382$ – $1389$  nm) may refer to stretching vibrations of B–OH groups, where boron is in triple coordination ( $\nu(\text{B}^{\text{III}}\text{–OH})$ ), as well as to bismuth active centers associated with silicon (BAC-Si) [20,23,25,26,28]. The bands at 7182–7158  $\text{cm}^{-1}$  ( $\sim 1392$ – $1397$  nm) may be associated with the absorption of hydroxyl groups and water molecules adsorbed on the surface, as well as with BAC-Si [20,23,25,26,28].

An additional weak band in a PG-NFF (Ar)-based BCM at 7749  $\text{cm}^{-1}$  ( $\sim 1291$  nm) is most likely associated with the absorption of water molecules adsorbed on the surface, including the modification of water  $\text{HD}^{16}\text{O}$ , and with centers  $\text{Bi}\cdots\equiv\text{Si}\text{–}\text{Si}\equiv$  in  $\text{SiO}_2$  (BAC-Si) [29,30]. The observed additional bands in BCM based on PG 8V-NT ( $\text{N}_2/\text{Ar}$ ) at 4185 ( $\sim 2390$ ) and 4180  $\text{cm}^{-1}$  ( $\sim 2392$  nm), as well as in QG-NFF and BCM based on PG-NFF (air) at 4182  $\text{cm}^{-1}$  ( $\sim 2391$  nm) are most likely associated with valence oscillations of OH groups ( $\nu(\text{OH})$ ) with low frequency lattice vibration [23] and with absorption of bismuth dimers  $\text{Bi}_2^+$  [31].

It should be noted, that there are no differences in the samples of BCM based on PG-8V-NT (Fig. 1, c) depending on the sintering atmosphere ( $\text{N}_2/\text{Ar}$ ). IR transmission spectra of QG 8V-NT, depending on the sintering atmosphere, do not differ from the spectrum of QG 8V-NT (air) according to [26].

Thus, the presence of additional bands is established in the BCM when 7749, 7238–7200, 7182–7158  $\text{cm}^{-1}$ , which are associated with the presence of bismuth active centers associated with silicon, and at 4185, 4182, 4180  $\text{cm}^{-1}$  — with absorption of bismuth dimers  $\text{Bi}_2^+$ .

Fig. 2 shows the excitation spectra of HCM luminescence depending on the sintering atmosphere ( $\text{N}_2/\text{Ar}$ ) and the type of PG-matrix (8V-NT, NFF). The position of the bands in the excitation spectra of red luminescence belonging to divalent bismuth ions in BCM, regardless of the presence of phosphate and fluoride ion impurities in them, is almost the same. The luminescence excitation spectra ( $\lambda_{\text{em}} = 600$  nm) clearly show bands at 240–250 (band edge), 350 and 465 nm (Fig. 2, a), and also bands at 240–250 (band edge), 310 ( $\text{N}_2$ ), 320 (Ar) and 465 nm (Fig. 2, b). However, the intensity of the bands on the excitation spectra of luminescence in samples of BCM based on PG-NFF is significantly higher (Fig. 2, b). At the same time, they are characterized by the appearance of additional clearly defined bands at 310 ( $\text{N}_2$ ) and 320 nm (Ar). Bands with highs of 240–250 (band edge) are described by the electronic transition  $^1S_0 \rightarrow ^1P_1$  of  $\text{Bi}^{3+}$  ions, and the bands at 310, 320, 350 nm belong to  $\text{Bi}^{\text{ions}3+}$  (electronic transition  $^1S_0 \rightarrow ^3P_1$ ), the band at 465 nm refers to the ions  $\text{Bi}^{2+}$  (electronic transition  $^2P_{1/2} \rightarrow ^3P_{3/2}(2)$ ) [32,33]. Similar results were found in the paper [4] in samples of BCM based on PG-8V-NT, heat-treated at 870°C in an air atmosphere.

A comparison of the luminescence excitation spectra of different BCM samples indicates that heat treatment (sintering) is preferable to obtain intense red luminescence BCM based on PG-NFF matrices in a nitrogen atmosphere. It follows from the data obtained that the PG-NFF matrix may be promising for obtaining active media with an increased proportion of bismuth active centers, assuming that the reduced form of bismuth [8] participates in the formation of active centers. Thus, it is established that in the PG-NFF matrix, the process of transformation of  $\text{Bi}^{3+}$  into  $\text{Bi}^{2+}$  occurs more efficiently than in the PG-8V-NT matrix (all other things being equal).

At  $\lambda_{\text{ex}} = 280$  nm samples of QG 8V-NT ( $870 \pm 10^\circ\text{C}$ , air atmosphere) emit in the region of 320 nm [4], and at  $\lambda_{\text{ex}} = 300$  nm samples of QG 8V-NT ( $890 \pm 10^\circ\text{C}$ , air atmosphere) emit in the UV region (band edge at  $\sim 350$  nm) [5]. UV luminescence at 320–350 nm may be associated with silicon defect centers ( $=\text{Si}^0$ ) in the silica matrix of glass (electronic transition  $S_1 \rightarrow S_0$ ) [5,34]. Luminescence in the specified range was not observed in composites based on PG-8V-NT.

Fig. 3 shows the luminescence spectra of QG NFF depending on the sintering atmosphere (air/ $\text{N}_2/\text{Ar}$ ) at  $\lambda_{\text{ex}} = 280$  nm and  $\lambda_{\text{ex}} = 380$  nm.

With  $\lambda_{\text{ex}} = 280$  nm for samples in the series of QG NFF ( $870 \pm 10^\circ\text{S}$ , air) — QG NFF ( $890 \pm 10^\circ\text{S}$ , Ar) — QG NFF ( $890 \pm 10^\circ\text{C}$ ,  $\text{N}_2$ ) luminescence bands are visible with maxima at 415, 435, 510 nm — 417, 436, 508 nm — 415, 435, 509 nm, respectively. The intensity of the luminescence bands in QG NFF ( $\text{N}_2$ ) is  $\sim 2$  times higher than in QG NFF (air/Ar). It is established that there are no changes in the nature of the luminescence spectra depending on the sintering atmosphere.

With an increase in the excitation wavelength at  $\lambda_{\text{ex}} = 380$  nm, luminescence bands were detected in samples of QG NFF ( $870 \pm 10^\circ\text{C}$ , air) — QG NFF ( $890 \pm 10^\circ\text{C}$ , Ar) — QG NFF ( $890 \pm 10^\circ\text{C}$ ,  $\text{N}_2$ ) with highs near 413, 435, 557 nm — 413, 437, 557, 566 nm — 405, 457, 557, 568 nm, respectively. The intensity of the luminescence bands in QG NFF ( $\text{N}_2$ ) is higher, and weak luminescence bands in the region of 550–570 nm are more clearly expressed.

Luminescence bands at 405–417 nm are most likely associated with an internal defect  $\text{O}_2^-$  (overview in [35]). The band at 457 nm (QG NFF,  $\text{N}_2$ ), it probably refers to SiODC centers (electronic transition  $T_1 \rightarrow S_0$ ) [34]. Narrow bands at 435–437 and 457 nm may be associated with defects  $\text{O}_3 \equiv \text{Si}\text{–}\text{Si}\equiv\text{O}_3$  [36]. The observed luminescence at 508–510 nm is associated with silicon defect centers ( $=\text{Si}^0$ ) in the silica matrix of glass (electronic transition  $T_1 \rightarrow S_0$ ) [34]. The weak band at 557 nm may be associated with a lack of oxygen or  $E'$  centers (positively charged oxygen vacancies) [36]. Bands at 566 and 568 nm ( $\sim 2.2$  eV) may refer to interstitial oxygen  $\text{O}_2^-$  or to the self-captured exciton [37].

It was previously found that at  $\lambda_{\text{ex}} = 380$  nm, samples of QG 8V-NT ( $870 \pm 10^\circ\text{C}$ , air) have luminescence in a wide

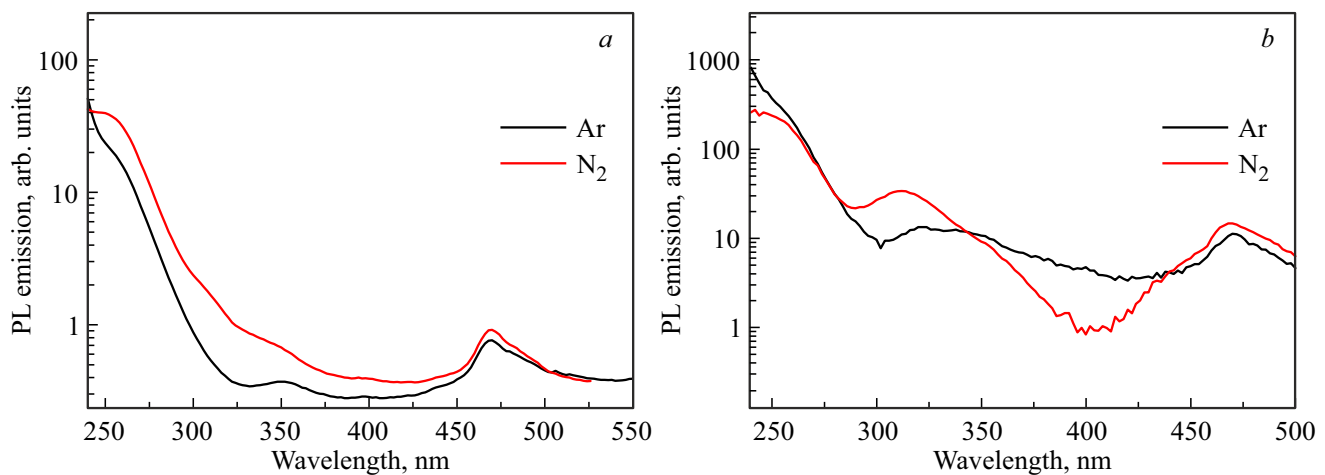


**Figure 2.** Luminescence excitation spectra of BCM (heat treatment at 900°C) depending on the sintering atmosphere (argon, nitrogen) and the type of matrix (*a* — PG-8V-NT, *b* — PG-NFF) ( $\lambda_{em} = 600$  nm,  $T = 300$  K).

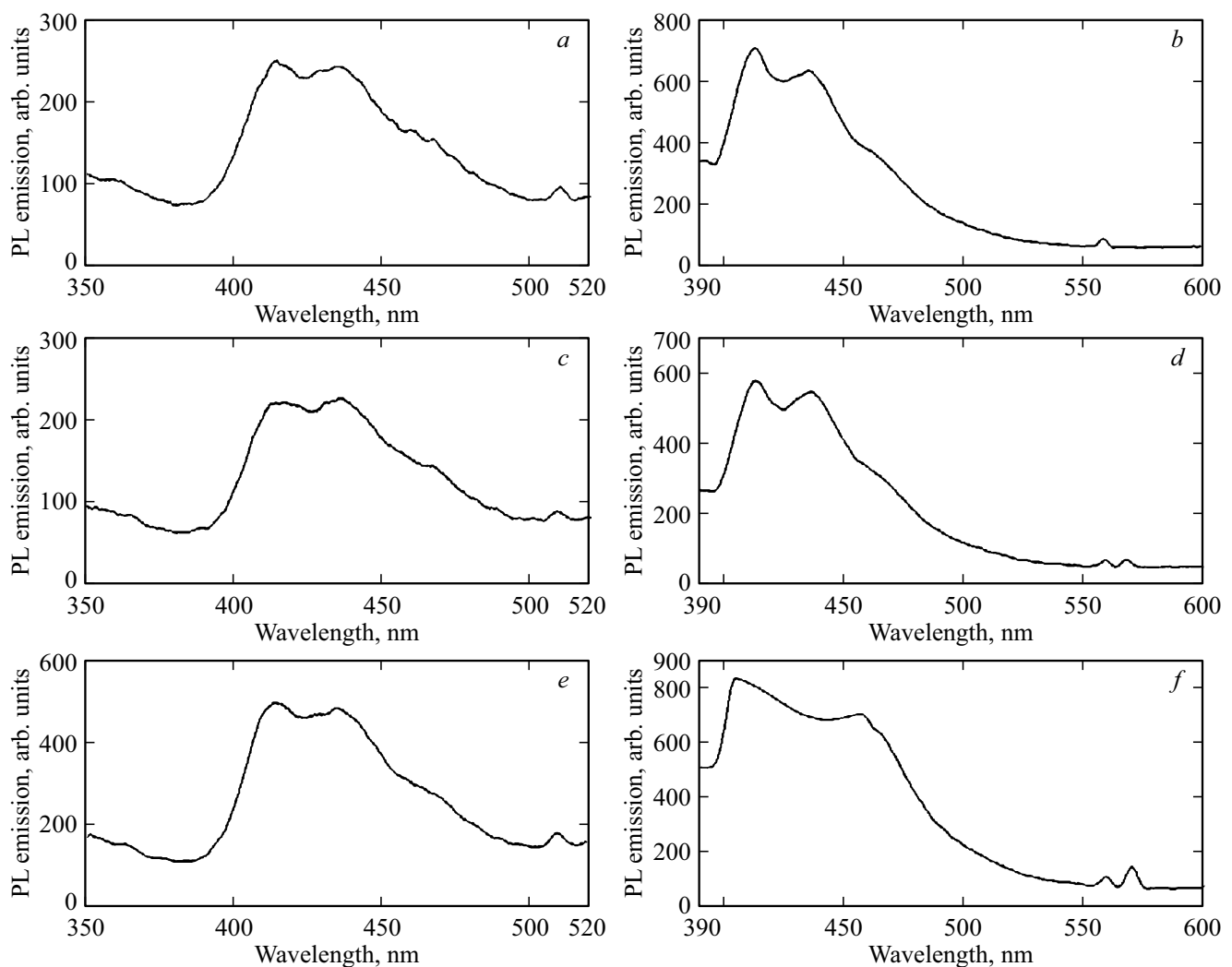


**Figure 3.** Luminescence spectra of QG-NFF (heat treatment at 870–900°C) depending on the sintering atmosphere: *a, b* — air; *c, d* — argon; *e, f* — nitrogen (*a, c, e* —  $\lambda_{ex} = 280$  nm,  $T = 300$  K; *b, d, f* —  $\lambda_{ex} = 380$  nm,  $T = 300$  K).

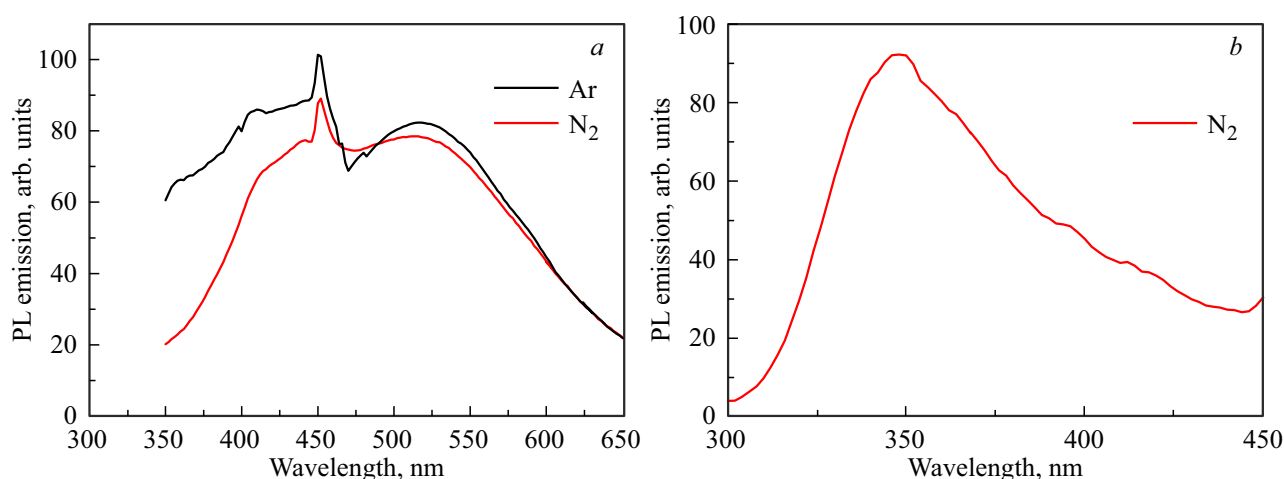


**Figure 4.** Luminescence spectra of BCM (heat treatment at 900°C) depending on the sintering atmosphere (argon, nitrogen) and the type of matrix (*a* — PG-8V-NT, *b* — PG-NFF) ( $\lambda_{\text{ex}} = 280$  nm,  $T = 300$  K).

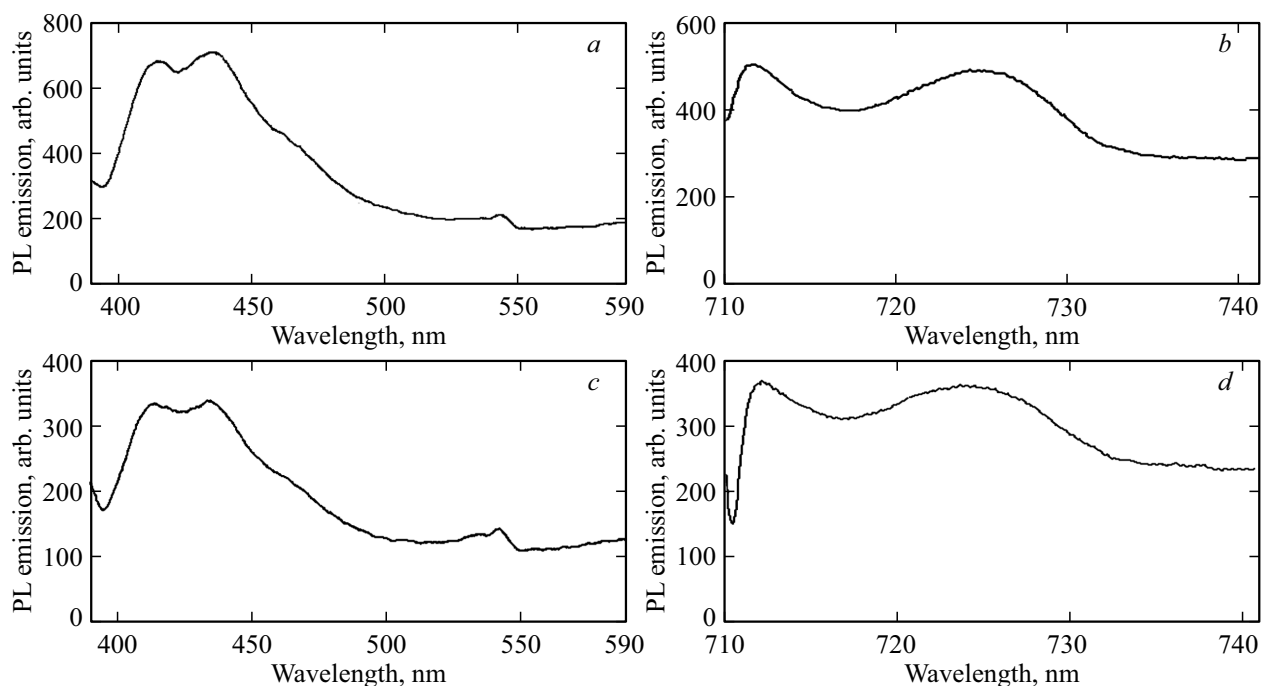


**Figure 5.** HCM luminescence spectra (heat treatment at 900°C; sintering atmosphere — nitrogen) depending on the type of matrix (*a, b* — PG-8V-NT, *c, d* — PG-NFF) ( $\lambda_{\text{ex}} = 350$  nm,  $T = 300$  K).

spectral range of 400–550 nm with a weak peak at 450 nm due to defects in the glass mesh (see overview in [38]).

Fig. 4 shows the luminescence spectra ( $\lambda_{\text{ex}} = 280$  nm) of BCM samples depending on the sintering atmosphere ( $\text{N}_2/\text{Ar}$ ) and the type of PG-matrix (8V-NT, NFF). It can be seen that two bands of about 450 and 510–550 nm (blue and green luminescence) can be observed in the BCM series based on PG-8V-NT (Fig. 4,*a*), which belong to one BAC ( $\text{Bi}^{3+}$  ions, electronic transition  $^3P_{1,0} \rightarrow ^1S_0$ ) [9,33,39]. The influence of the sintering atmosphere is not observed. At the same time, luminescence in the near UV region is characteristic for samples

of BCM based on PG-NFF ( $\text{N}_2$ ) — a band of about 350 nm can be observed on the spectrum (Fig. 4,*b*), which corresponds to the electronic transition of  $^3P_{1,0} \rightarrow ^1S_0$  ions  $\text{Bi}^{3+}$  [10,14,33,40].

When comparing Fig. 4 and 5 ( $\lambda_{\text{ex}} = 350$  nm), it is seen that with an increase in the excitation wavelength ( $\lambda_{\text{ex}} = 350$  nm) in the luminescence spectra of BCM depending on of the PG-matrix type (8V-NT, NFF), there are no differences in the shape of the BCM luminescence spectra and the position of the luminescence bands, but only the intensity of the luminescence changes. Bands of blue-green and red luminescence were detected with

maxima near 415, 435, 543, 712 and 725 nm (BCM based on PG-8V-NT) and 413, 433, 543, 712 and 725 nm (BCM based on PG-NFF). The blue-green luminescence bands correspond to the electronic transition  ${}^3P_{0,1} \rightarrow {}^1S_0$  of  $\text{Bi}^{3+}$  [4,5,9,14,18,32,33]. The red luminescence bands at 712 and 725 nm are associated with the electronic transition  ${}^3P_2 \rightarrow {}^3P_0$  of  $\text{Bi}^{3+}$  ions and with the electronic transition  ${}^3P_{3/2}(1) \rightarrow {}^2P_{1/2}$  ions  $\text{Bi}^{2+}$  [5,10,14,18,33,40,41].

Thus, the higher efficiency of converting  $\text{Bi}^{3+}$  into  $\text{Bi}^{2+}$  ions in composites based on the PG-NFF matrix compared to the PG-8V-NT matrix may be related to the existing structural differences of the matrices. Indirectly, this assumption follows from a comparison of the luminescence excitation spectra (Fig. 2).

## Conclusion

Samples of bismuth-containing composite materials (BCM) based on matrices of high-silica porous glasses were synthesized, which were subjected to heat treatment in an atmosphere of nitrogen or argon at  $890 \pm 10^\circ\text{C}$  for 15 min.

Studies of bismuth-containing composite materials by near-IR spectroscopy revealed the presence of bismuth active centers associated with silicon and bismuth dimers  $\text{Bi}_2^+$ .

It is shown that bismuth-containing composite materials have UV, blue-green and orange-red luminescence, which is associated with the presence of various bismuth active centers (ions  $\text{Bi}^{3+}$ ,  $\text{Bi}_2^+$  and  $\text{Bi}^+$ ) in composites.

It is established that in the PG-NFF matrix, the process of transformation of  $\text{Bi}^{3+}$  into  $\text{Bi}^{2+}$  occurs more efficiently than in the PG-8V-NT matrix (other things being equal). Therefore, in order to obtain intense red luminescence of BCM, it is preferable to use PG-NFF matrices and conduct heat treatment (sintering) BCM in a nitrogen atmosphere.

Experimental confirmation has been obtained that the process of reduction of  $\text{Bi}^{3+}$  ions in synthesized BCM significantly depends simultaneously on the chemical composition of the matrix, as well as on temperature conditions and redox conditions of processing composites.

## Acknowledgment

The authors are grateful to Dr. S.V. Firstov, an employee of the National Research Center of the Russian Academy of Sciences, for measuring the luminescence and luminescence excitation spectra of samples using an optical spectrofluorimeter FLS920 (Edinburgh Instruments).

## Funding

The work was carried out as part of the State assignment of the IHS RAS with the support of the Ministry of Education and Science of Russia (State registration № 1021050501068-5-1.4.3 (FFEM-2022-0004 project)).

## Conflict of interest

The authors declare that they have no conflict of interest.

## References

- [1] D. Zhang, S. Wang, Y. Liu, W. Su, N. Zhang, Z. Liu, Z. Wang, L. Yang, J. Qiu. *Ceramics International*, **47** (23), 32619 (2021). DOI: 10.1016/j.ceramint.2021.08.157
- [2] S. Xiang, M. Zhang, T. Zeng, J. Chen, F. Zhang. *Micromachines*, **13** (6), 921 (2022). DOI: 10.3390/mi13060921
- [3] M.L. Krishnan, M.M. Neethish, V.V. Ravi Kanth Kumar. *J. Lumin.*, **201**, 442 (2018). DOI: 10.1016/j.jlumin.2018.05.023
- [4] S.V. Firstov, M.A. Girsova, E.M. Dianov, T.V. Antropova. *Glass Physics and Chemistry*, **40** (5), 521 (2014). DOI: 10.1134/S1087659614050046.
- [5] M.A. Girsova, S.V. Firstov, T.V. Antropova. *Glass Physics and Chemistry*, **45** (2), 98 (2019). DOI: 10.1134/S1087659619020068.
- [6] T.V. Antropova, M.A. Girsova, I.N. Anfimova, G.F. Golovina, L.N. Kurylenko, S.V. Firstov. Patent of the RF № 2605711 (2016).
- [7] M.A. Girsova, S.V. Firstov, I.N. Anfimova, G.F. Golovina, L.N. Kurylenko, T.G. Kostyreva, I.G. Polyakova, T.V. Antropova. *Fiz. Khim. Stekla*, **38** (S6), 861 (2012). (in Russian).
- [8] M.A. Girsova, T.V. Antropova, I.N. Anfimova, G.F. Golovina, L.N. Kurylenko. Patent RF na izobretenie № 2022113023; zayavl. 13.05.2022. (in Russian).
- [9] S. Zhou, N. Jiang, B. Zhu, H. Yang, S. Ye, G. Lakshminarayana, J. Hao, J. Qiu. *Advanced Functional Materials*, **18** (9), 1407 (2008). DOI: 10.1002/adfm.200701290
- [10] E.G. Firstova, I.A. Bufetov, V.F. Khopin, V.V. Vel'miskin, S.V. Firstov, G.A. Bufetova, K.N. Nishchev, A.N. Gur'yanov, E.M. Dianov. *Quantum Electronics*, **45** (1), 59 (2015). DOI: 10.1070/QE2015v045n01ABEH015624.
- [11] E.H. Sekiya, K. Saito. *Key Engineering Materials*, **702**, 91 (2016). DOI: 10.4028/www.scientific.net/kem.702.91
- [12] I.A. Bufetov, S.L. Semenov, V.V. Vel'miskin, S.V. Firstov, G.A. Bufetova, E.M. Dianov. *Quantum Electronics*, **40** (7), 639 (2010). DOI: 10.1070/QE2010v040n07ABEH014350.
- [13] R. Wan, Z. Song, Y. Li, Y. Zhou, Q. Liu, J. Qiu, Z. Yang, Z. Yin. *J. Appl. Phys.*, **117**, 053107 (2015). DOI: 10.1063/1.4907565
- [14] H.K. Dan, A.-L. Phan, N.M. Ty, D. Zhou, J. Qiu. *Optical Materials*, **112**, 110762 (2021). DOI: 10.1016/j.optmat.2020.110762
- [15] L.D. Iskhakova, V.M. Mashinsky, F.O. Milovich, V.V. Vel'miskin, E.A. Plastinin, S.V. Firstov, M.V. Lukashova, P.A. Somov, E.M. Dianov. *J. Non-Crystalline Solids*, **503–504**, 28 (2019). DOI: 10.1016/j.jnoncrysol.2018.09.022
- [16] D.N. Vtyurina, A.N. Romanov, K.S. Zaramenskikh, M.N. Vasil'eva, Z.T. Fattakhova, L.A. Trusov, P.A. Loiko, V.N. Korchak. *Russ. J. Physical Chemistry B*, **10** (2), 211 (2016). DOI: 10.1134/S1990793116020123.

- [17] S.V. Firstov, V.F. Khopin, I.A. Bufetov, E.G. Firstova, A.N. Guryanov, E.M. Dianov. *Optics Express*, **19** (20), 19551 (2011). DOI: 10.1364/OE.19.019551
- [18] B. Xu, D. Tan, S. Zhou, Z. Hong, K.N. Sharafudeen, J. Qiu. *Optics Express*, **20** (27), 29105 (2012). DOI: 10.1364/OE.20.029105
- [19] H.El. Hamzaoui, C. Kinowski, I. Razdobreev, A. Cassez, G. Bouwmans, B. Prochet, B. Capoen, M. Bouazaoui. *Physica Status Solidi A*, **216** (3), 1800411 (2019). DOI: 10.1002/pssa.201800411
- [20] E.M. Dianov. *Light: Science & Applications*, **1**, e12 (2012). DOI: 10.1038/lssa.2012.12
- [21] X. Jiang, A. Jha. *Optical Materials*, **33** (1), 14 (2010). DOI: 10.1016/j.optmat.2010.07.011
- [22] V.M. Denisov, N.V. Belousova, G.K. Moiseev, S.G. Bakhvalov, S.A. Istomin, E.A. Pastukhov. *Bismuth-containing materials: structure and physico-chemical properties* (Ural Branch of the Russian Academy of Sciences, Yekaterinburg, 2000), pp. 422–443.
- [23] M.A. Girsova, G.F. Golovina, L.N. Kurilenko, I.N. Anfimova. *Glass Physics and Chemistry*, **46** (6), 531 (2020). DOI: 10.1134/S1087659620060085.
- [24] M.A. Girsova, L.N. Kurilenko, I.N. Anfimova, M.Yu. Arsent'ev, L.F. Dikaya, E.A. Semenova. *Russian Chemical Bulletin*, **69** (5), 920 (2020). DOI: 10.1007/s11172-020-2849-9.
- [25] M.A. Girsova, G.F. Golovina. *Glass Physics and Chemistry*, **44** (6), 569 (2018). DOI: 10.1134/S1087659618060068.
- [26] M.A. Girsova, G.F. Golovina, I.N. Anfimova, L.N. Kurilenko. *Glass Physics and Chemistry*, **44** (5), 381 (2018). DOI: 10.1134/S1087659618050061.
- [27] D.P. Zarubin. *Physics and Chemistry of Glasses*, **40** (4), 184 (1999).
- [28] A.V. Kir'yanov, S.H. Siddiki, Y.O. Barmenkov, D. Dutta, A. Dhar, S. Das, M.C. Paul. *Optical Materials Express*, **7** (10), 3548 (2017). DOI: 10.1364/OME.7.003548
- [29] V.O. Sokolov, V.G. Plotnichenko, E.M. Dianov. *Optical Materials Express*, **3** (8), 1059 (2013). DOI: 10.1364/OME.3.001059
- [30] R.A. Toth. *J. Molecular Spectroscopy*, **186** (1), 66 (1997). DOI: 10.1006/jmsp.1997.7398
- [31] V.G. Plotnichenko, V.O. Sokolov, D.V. Philippovskiy, I.S. Lisitsky, M.S. Kouznetsov, K.S. Zaramenskikh, E.M. Dianov. *Opt. Lett.*, **38** (3), 362 (2013). DOI: 10.1364/OL.38.000362
- [32] J.F. Liu. *Optik*, **126** (23), 4115 (2015). DOI: 10.1016/j.jjleo.2015.07.207
- [33] M. Puchalska, E. Zych, P. Bolek. *J. Alloys and Compounds*, **806**, 798 (2019). DOI: 10.1016/j.jallcom.2019.07.307
- [34] V.O. Sokolov, V.B. Sulimov. *Physica Status Sol. B*, **186** (1), 185 (1994). DOI: 10.1002/pssb.2221860115
- [35] M.A. García, S.E. Paje, M.A. Villegas, J. Llopis. *Materials Lett.*, **43** (1–2), 23 (2000). DOI: 10.1016/S0167-577X(99)00224-4
- [36] J.A.L. López, J.C. López, D.E.V. Valerdi, G.G. Salgado, T. Díaz-Becerril, A.P. Pedraza, F.J.F. Gracia. *Nanoscale Research Lett.*, **7**, 604 (2012). DOI:10.1186/1556-276x-7-604
- [37] A.J. Miller, R.G. Leisure, V.A. Mashkov, F.L. Galeener. *Phys. Rev. B*, **53** (14), R8818 (1996). DOI: 10.1103/physrevb.53.r8818
- [38] T.V. Antropova, M.A. Girsova, I.N. Anfimova, I.A. Drozdova. *J. Lumin.*, **193**, 29 (2018). DOI: 10.1016/j.jlumin.2017.09.005
- [39] F. Kang, M. Peng. *Dalton Transactions*, **43**, 277 (2014). DOI: 10.1039/c3dt51183a
- [40] W. Wang, C. Jiang. *J. Alloys and Compounds*, **820**, 153169 (2020). DOI: 10.1016/j.jallcom.2019.153169
- [41] R. Cao, F. Zhang, C. Liao, J. Qiu. *Optics Express*, **21** (13), 15728 (2013). DOI: 10.1364/OE.21.015728